

Cite this paper: *Chin. J. Chem.* 2021, 39, 2113–2118. DOI: 10.1002/cjoc.202000695

# Uniform Formation of Amorphous Cobalt Phosphate on Carbon Nanotubes for Hydrogen Evolution Reaction<sup>†</sup>

 Mengzhan Ge,<sup>‡,a</sup> Xiaodong Zhang,<sup>‡,a</sup> Shangzhou Xia,<sup>b</sup> Wenjie Luo,<sup>a</sup> Yuwei Jin,<sup>a</sup> Qianqian Chen,<sup>a</sup> Huagui Nie<sup>\*,a</sup> and Zhi Yang<sup>\*,a</sup>
<sup>a</sup> Key Laboratory of Carbon Materials of Zhejiang Province, College of Chemistry and Materials Engineering, Wenzhou University, Wenzhou, Zhejiang 325027, China

<sup>b</sup> AECC Hunan Aviation Powerplant Research Institute, Zhuzhou, Hunan 412002, China

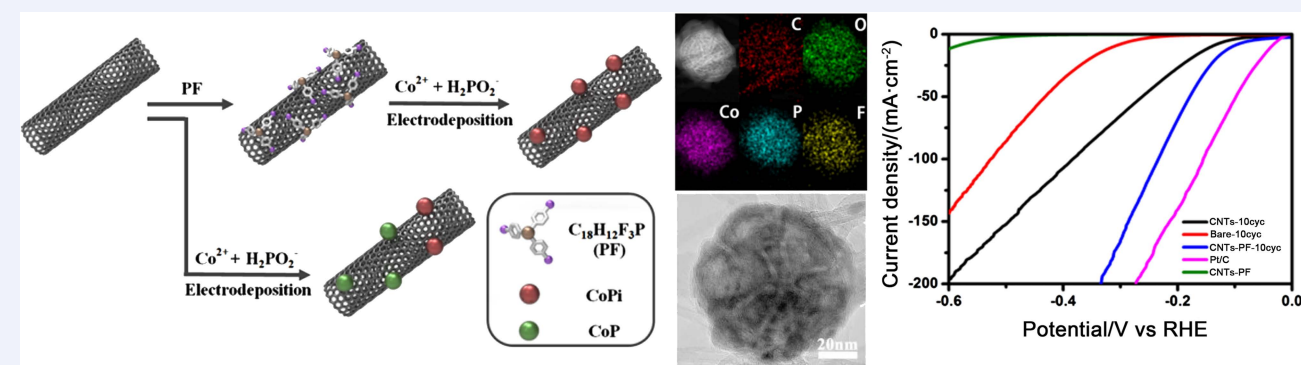
## Keywords

Cobalt phosphate | Heterogeneous catalysis | Carbon nanotubes | Electrochemistry | Water splitting

## Main observation and conclusion

Tremendous efforts have been made to the development of highly active, stable hydrogen evolution reaction (HER) electrocatalysts based on earth-abundant metal compounds. Recently, cobalt phosphorus (Co-P) catalysts have received particular attention owing to their good performances for the HER. However, the reported Co-P catalysts were not uniformly anchored on the substrates. Hence, developing Co-P catalysts with a uniform surface structure for HER remains a major challenge. Herein, we utilized small molecule tris-(4-fluorophenyl)phosphane (PF) for preliminarily functionalizing carbon nanotubes (PF-CNTs) via  $\pi$ - $\pi$  stacking interactions. Using these as the substrate, amorphous cobalt phosphate (CoPi) catalysts could then be uniformly anchored on PF-CNTs by electrodeposition method. These obtained CoPi/PF-CNTs catalysts show an onset potential low to 29 mV, a low overpotential (105 mV in 0.5 mol/L H<sub>2</sub>SO<sub>4</sub> at a current density of 10 mA·cm<sup>-2</sup> with a Tafel plot of 32 mV·dec<sup>-1</sup>) and an excellent stability for HER in acidic electrolyte, which is a promising noble-metal-free HER catalyst.

## Comprehensive Graphic Content


<sup>\*</sup>E-mail: huaguinie@126.com; yang201079@126.com

<sup>‡</sup>These authors contributed equally to this work.

<sup>†</sup>Dedicated to the Special Issue of Nanostructured Materials for Electrochemical Energy Conversion and Storage

[View HTML Article](#)
[Supporting Information](#)

## Background and Originality Content

Hydrogen, a green and renewable energy source, is considered as a potential alternative to traditional fuels like coal, oil, and natural gas.<sup>[1–3]</sup> Recently, one of the most promising approaches to generate H<sub>2</sub> is electrochemical water splitting due to its low-cost and high-efficiency.<sup>[4–5]</sup> Pt-based materials are routinely used as electrocatalysts owing to their high catalytic activity for hydrogen evolution reaction (HER) during the process of electrochemical water splitting.<sup>[6–8]</sup> Unfortunately, such precious-metal catalysts are scarce and expensive, which seriously hinder their applications in HER.<sup>[9–10]</sup> Therefore, it is imperative to design and fabricate an alternative, highly efficient and low-cost HER catalyst.<sup>[11–14]</sup>

In recent years, tremendous efforts have been focused on earth-abundant metal compounds as promising candidate electrocatalysts to produce highly active, stable HER performances.<sup>[15–19]</sup> Among these compounds, cobalt phosphorus (Co-P) compounds catalysts have attracted wide interest in HER due to their intrinsic rich coordinatively unsaturated atoms by theoretical calculations.<sup>[20–25]</sup> Very recently, various Co-P catalysts have demonstrated their great potential as highly-efficient HER catalysts.<sup>[20,26–30]</sup> These catalysts were prepared by various methods including electrodeposition, solvothermal methods, and chemical vapor deposition.<sup>[31–33]</sup> Among these methods, electrodeposition methods are intriguing due to low cost, ease of operation, and simple instrumentation. For instance, some groups have utilized electrodeposition methods to successfully synthesize cobalt phosphide (CoP) catalysts on carbon nanotubes (CNTs) substrates through POx groups in CoP.<sup>[21,34–35]</sup> However, the obtained Co-P catalysts could not be uniformly anchored on the CNTs substrates, attributed to the heterogeneous growth way of Co-P catalysts on CNTs. Moreover, the inherent diversity of CNTs from surface defects and five- or seven-membered-rings heavily hampered the uniformity of the CNTs.<sup>[36–37]</sup> Up to now, it remains a major challenge to obtain Co-P catalysts with a uniform surface structure on CNTs as highly-efficient HER electrocatalysts. Therefore, it is extremely urgent to develop a novel electrodeposition method to solve these problems.

Herein, we utilized a facile electrodeposition method to prepare the catalysts. The corresponding synthetic procedure is illustrated in Figure 1. Small molecule tris(4-fluorophenyl)phosphine (PF, its structure shown in Figure S1 in Supporting Information) was used to preliminarily functionalize CNTs via  $\pi$ - $\pi$  stacking interactions to obtain the uniform CNTs phosphates (PF-CNTs). P atoms in PF exhibit smaller electronegativity (electronegativity of phosphorus: 2.19) with respect to C atoms (electronegativity of carbon: 2.55), which leads to the creating of positive charge density on P atoms.<sup>[38]</sup> These factors can facilitate H<sub>2</sub>PO<sub>4</sub><sup>-</sup> and OH<sup>-</sup> in electrolyte to favorably adsorb and accumulate onto electrodes. Therefore, more O atoms can participate in the following electrodeposition process and lead to the uniform formation of amorphous cobalt phosphate (CoPi) onto the CNTs-PF substrates.

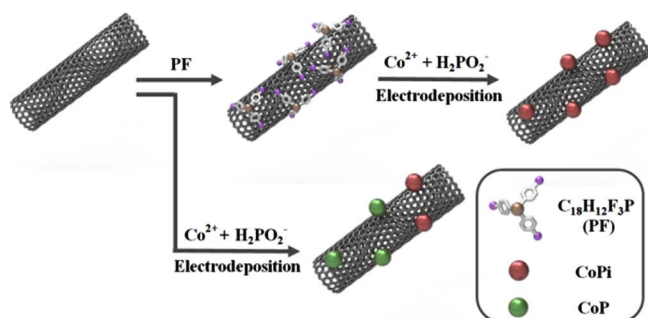


**Figure 1** A schematic diagram to illustrate the synthetic procedure of the CoPi/PF-CNTs nanocomposites.

Whereas, the absence of PF could not induce more O atoms to accumulate onto the surface of the electrode, thus producing the composites of CoP and CoPi. The catalysts benefit from a high bonding strength with the substrate, less interfacial resistance, and an increased catalytic activity area. The obtained CoPi/PF-CNTs catalysts show a low onset potential of 29 mV vs RHE, an overpotential of 105 mV at a current density of 10 mA·cm<sup>-2</sup>, excellent stability under acidic conditions, and a Tafel slope of 32 mV·dec<sup>-1</sup> (comparable to that of Pt/C). Overall, the CoPi/PF-CNTs catalysts show impressive HER performances under acidic environments.

## Results and Discussion

The CoPi/PF-CNTs nanocomposites were synthesized via a facile electrochemical process. In a typical experiment, PF was first uniformly distributed on the surface of CNTs through  $\pi$ - $\pi$  stacking interactions. Subsequently, the obtained PF-CNTs-modified glassy carbon electrodes (GCEs) were performed in a mixture of CoSO<sub>4</sub>·7H<sub>2</sub>O, NaH<sub>2</sub>PO<sub>2</sub>·H<sub>2</sub>O, and H<sub>3</sub>BO<sub>3</sub> aqueous solutions through cyclic voltammogram (CV) with 5, 10, 20 cycles, respectively. The obtained CoPi/PF-CNTs nanocomposites were denoted as CNTs-PF-5cyc, CNTs-PF-10cyc, and CNTs-PF-20cyc, respectively. For comparison, the CNTs-modified GCEs without PF were directly treated under the same electrolyte solution through CV with 5, 10, 20 cycles, respectively. The corresponding catalysts were denoted as CNTs-5cyc, CNTs-10cyc, and CNTs-20cyc, respectively.

The scanning electron microscopy (SEM) images of CNTs-PF-10cyc in Figure 2a clearly demonstrate that the CoPi nanospheres were uniformly interspersed across CNTs networks. Transmission electron microscopy (TEM) images (Figures 2b,c) show that these nanospheres were closely attached to the CNTs and there were some porous structures present within the microspheres. The scanning transmission electron microscopy (STEM) and corresponding elemental mappings in Figure 2d show a uniform spatial distribution of the nanoparticles with Co, O, P, and F atoms for CNTs-PF-10cyc catalyst. For the control sample CNTs-10cyc, there is no F atom in the element mapping (Figure S2 in Supporting Information). These results indicated that CoPi was successfully grown on PF-CNTs. X-ray photoelectron spectroscopy (XPS) was further used to investigate the chemical composition and bonding configuration of the obtained CoPi/PF-CNTs nanocomposites. The survey spectrum of CNTs-PF-10cyc (Figure 3a) contained C1s, O1s, Co2p, P2p, and F1s peaks, confirming the presence of these elements. As shown in Figure 3b, the P2p region of CNTs-PF-10cyc exhibits its only sharp peak at 134.0 eV, which corresponds to the 2p<sub>1/2</sub> core level of a central P atom in a phosphate species. Elsewhere, the peak at 129.4 eV for

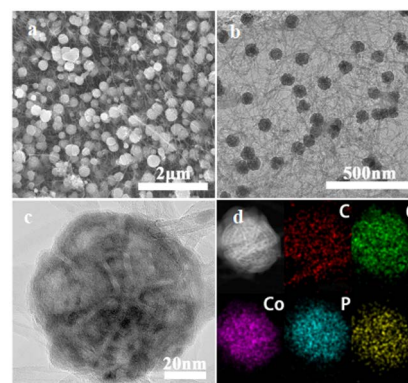


**Figure 2** Characterizations of the CNTs-PF-10cyc catalyst: (a) SEM image, (b, c) TEM images, and (d) STEM and the corresponding element mapping.

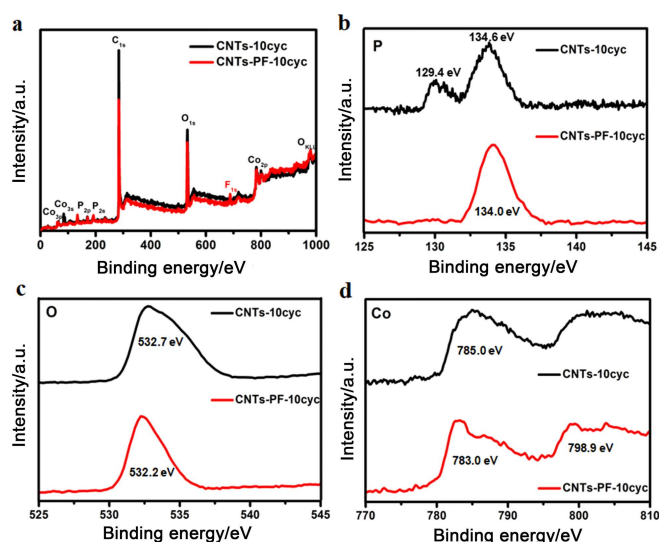


**Figure 3** XPS spectra characterizations: (a) survey spectrum, (b) P2p spectrum, (c) O1s spectrum, and (d) Co2p spectrum.

CNTs-10cyc reflects the binding energies (BEs) of P2p<sub>1/2</sub>, which can be assigned to the phosphide group.<sup>[22,39-40]</sup> These XPS results confirm that PF can induce more O atoms onto the electrode and lead to the oxidation of P atom into phosphate species, which lead to the formation of the nearly pure CoPi catalysts on the PF-modified CNTs through electrodeposition method. Furthermore, combing with TEM, XPS, and SAED results (Figure S3 in Supporting Information), it can be obtained that the CNTs-PF-10cyc catalyst with pure CoPi is amorphous. These similar phenomena could also be found in the reported literatures.<sup>[22,34-35]</sup> Moreover, compared with that of CNTs-10cyc, the O1s peak of CNTs-PF-10cyc showed a shift of ~0.5 eV to a lower BE (Figure 3c). In the Co region of the CNTs-PF-10cyc (Figure 3d), the two broad set of signals corresponding to 2p<sub>3/2</sub> (783.0 eV) and 2p<sub>1/2</sub> (798.9 eV) core levels can be considered to reflect the Co<sup>2+</sup> oxidation state.<sup>[22]</sup> Compared with that of CNTs-10cyc, the variation of O1s and Co2p peak positions for the CNTs-PF-10cyc may be attributed to their different electron states of P originating from that P atom with smaller electronegativity would lose more electron and lead to the increase of electron density around the adjacent Co atoms and O atoms.<sup>[38]</sup>

The HER activities of the CoPi/PF-CNTs nanocomposites were evaluated in 0.5 mol/L H<sub>2</sub>SO<sub>4</sub> solution with a typical three-electrode configuration. Herein, GCEs modified with a constant mass loading of CNTs-PF-20cyc, CNTs-PF-10cyc, CNTs-PF-5cyc, CNTs-PF, CNTs-10cyc and bare GCE-10cyc, and 20 wt% Pt/C were used as the working electrodes, respectively. From Figure 4a, it can be obtained that the CNTs-PF-10cyc catalyst exhibited the most positive overpotential and the highest catalytic current among the prepared catalysts. Moreover, using a typical reference metric for electrochemical catalytic performance for HER, CNTs-PF-10cyc achieved an onset potential as small as 29 mV (Table 1) and the

current densities of 2 and 10 mA·cm<sup>-2</sup> yielded overpotentials of 46 and 105 mV, respectively. These were comparable to those of the reported catalysts for Pt-free HER (Table S1 in Supporting Information). Tafel slopes derived from polarization curves were further utilized to evaluate the activity of the prepared catalysts for HER, as shown in Figures 4b and 4c. The Tafel slope of CNTs-PF-10cyc catalyst was 32 mV·dec<sup>-1</sup>, which is similar to that of Pt/C catalyst (30 mV·dec<sup>-1</sup>). But, it was lower than that of the CNTs-10cyc (78 mV·dec<sup>-1</sup>). Moreover, this Tafel slope of CNTs-PF-10cyc catalyst is also superior to those of the reported Pt-free HER catalysts (Table S1 in Supporting Information). The value of the Tafel slope (32 mV·dec<sup>-1</sup>) suggested that the recombination of hydrogen was the rate-limiting step in the HER at low overpotentials.<sup>[41]</sup> According to the Tafel equation, exchange current densities in Table 1 were also determined by fitting the polarization data. The CNTs-PF-10cyc electrode exhibited a remarkable exchange current density of 1.78 × 10<sup>-2</sup> mA·cm<sup>-2</sup>, which is better than those of CNTs-10cyc and most non-Pt catalysts (Table S1 in Supporting Information). These results suggested excellent catalytic activity of CNTs-PF-10cyc for HER, which may be attributed to that PF molecule can effectively regulate the uniform formation of amorphous CoPi on CNTs and thus expose more catalytic activity sites for HER.

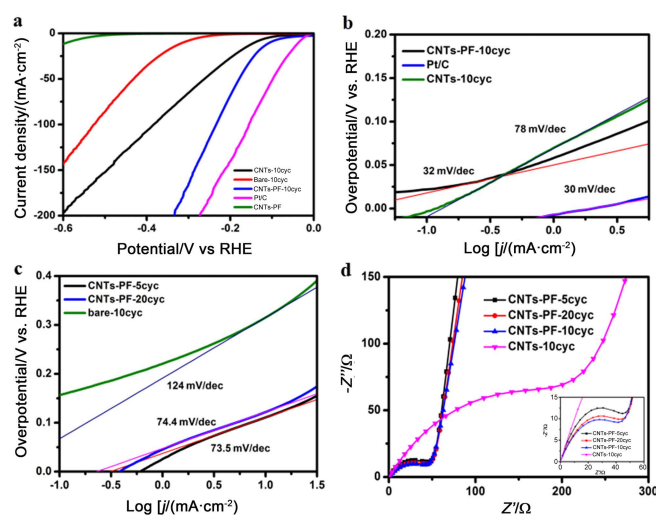


**Figure 4** Electrochemical characterizations of the hybrid catalysts: (a) Polarization curves of CNTs-10cyc, CNTs-PF-10cyc, CNTs-PF, Bare-10cyc, and Pt/C in 0.5 mol/L H<sub>2</sub>SO<sub>4</sub> solution; (b) Tafel plots of CNTs-PF-10cyc, CNTs-10cyc, and Pt/C; (c) Tafel plots of CNTs-PF-5cyc, CNTs-PF-20cyc, and Bare-10cyc; (d) Nyquist plots show the CNTs-PF-5cyc, CNTs-PF-10cyc, CNTs-PF-20cyc, and CNTs-10cyc, the inset displays Nyquist plots at high-frequency range.

In order to obtain the optimal CoPi/PF-CNTs electrocatalyst for HER, electrochemical deposition cycles and the mass ratio of CNTs to PF were systematically investigated in 0.5 mol/L H<sub>2</sub>SO<sub>4</sub> solution.

**Table 1** Comparison of HER performances of different catalysts

Sample	Onset potential/mV	$\eta_2$ /mV	$\eta_{10}$ /mV	Tafel slope/(mV·dec <sup>-1</sup> )	Exchange current density/(mA·cm <sup>-2</sup> )	Capacitance/(μF·cm <sup>-2</sup> )
CNTs-PF-5cyc	74	85	143	73.5	8.91 × 10 <sup>-4</sup>	9.95
CNTs-PF-10cyc	29	46	105	32.0	1.78 × 10 <sup>-2</sup>	14.38
CNTs-PF-20cyc	68	73	114	74.4	7.08 × 10 <sup>-4</sup>	12.52
CNTs-10cyc	56	59	141	78.0	5.01 × 10 <sup>-4</sup>	5.16
Bare-10cyc	205	235	312	124	3.55 × 10 <sup>-4</sup>	—
CNTs-PF	460	496	589	132	3.20 × 10 <sup>-7</sup>	4.08

It could be obtained from Figure S4 in Supporting Information that too much deposition cycles lead to the formation of larger CoPi agglomerations and too less deposition cycles lead to the limited formation of CoPi, which dramatically decreased the catalytic activity of the produced CoPi/PF-CNTs (Figure 4c and Figure S5 in Supporting Information). To further reveal the effect of the electrochemical deposition cycles on HER performance, an electrochemical impedance spectroscopy (EIS) analysis was performed in  $\text{H}_2\text{SO}_4$  for the CoPi/PF-CNTs catalysts. Nyquist plots were shown in Figure 4d. The low charge transfer resistance ( $R_{ct}$ ) value indicated a faster surface charge transfer and a higher reaction rate during electrocatalysis.<sup>[43]</sup> CNTs-PF-10cyc exhibited the lowest  $R_{ct}$  value among all of the CoPi/PF-CNTs catalysts (Figure S6 and Table S2 in Supporting Information). However, the CNTs-PF-5cyc catalyst with a higher  $R_{ct}$ , displayed the lowest catalytic activity for HER. Increasing the amount of cycles resulted in increased  $R_{ct}$ , attributed to the formation of larger CoPi agglomerations and decreased active sites for HER. Similar experimental phenomenon also appeared in CoPi/PF-CNTs catalysts with different mass ratios of CNTs to PF (Figure S7 in Supporting Information). When the mass ratio of CNTs to PF was 3 : 1, the optimal performance for HER was obtained. These results demonstrated that CNTs-PF-10cyc catalyst with 3 : 1 mass ratio of CNTs to PF showed the highest HER activity among all of the prepared CoPi/PF-CNTs catalysts.

The stability of CNTs-PF-10cyc was investigated through chronoamperometry measurements in acidic electrolytes. From Figure 5 and Figure S8 in Supporting Information, it can be obtained that the current of CNTs-PF-10cyc-modified electrode for HER showed a very little change during 24 h. Moreover, the batch-to-batch reliability was estimated from the current responses of five electrodes separately prepared under the same conditions toward HER, and a RSD of 10.2% was obtained. This exceptional long-term durability was superior to that of Pt/C (Figure S9 in Supporting Information), which suggested high stability and high reliability of the CNTs-PF-10cyc catalyst for HER.

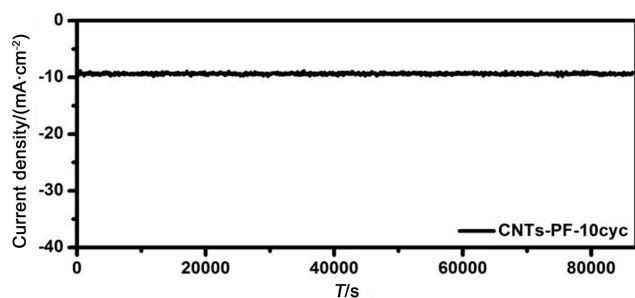


**Figure 5** Chronoamperometry curve of CNTs-PF-10cyc at  $\eta = 100$  mV in  $0.5$  mol/L  $\text{H}_2\text{SO}_4$ .

In order to figure out the reason why the CNTs-PF-10cyc catalysts exhibit the optimal performance for HER, the catalysts were further characterized by HRTEM. From Figures 6a and 6b, the CNTs-PF-10cyc revealed a wealth of interwoven macropores and micropores. The internal void space was made of across and longitudinal staggered channels. By comparison, the CNTs-10cyc catalyst clearly displayed a small number of capillary cracks and there was no longitudinal void structure in Figures 6c and 6d. Furthermore, the electrochemical surface area (ECSA) was evaluated for insight into the internal structure of the catalysts under different working conditions. The double-layer capacitance was calculated from CV curves at various scan rates between 0 and  $0.3$  V vs. RHE (Figure S10 in Supporting Information). From the slopes obtained from Figures 6e and 6f, the capacitances of CNTs-PF-10cyc and CNTs-10cyc were  $14.38$  and  $5.16$   $\text{mF}\cdot\text{cm}^{-2}$ , respectively. These results also agreed well with the corresponding HRTEM observa-

tions. The high degree of porosity increased the surface area and provided numerous active sites for ion/mass diffusion, significantly enhancing the electrochemical performance for HER.

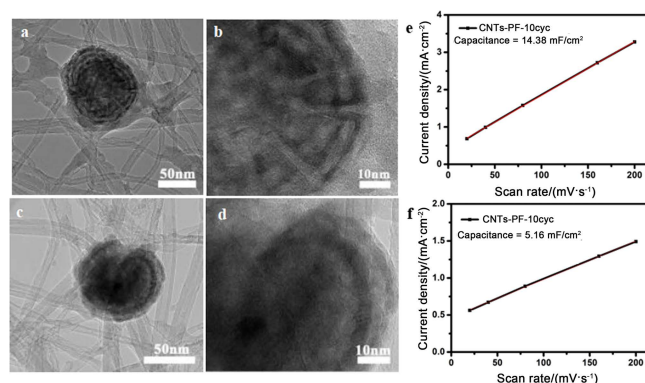


**Figure 6** HRTEM images of CNTs-PF-10cyc (a, b) and CNTs-10cyc (c, d); Double-layer capacitances of CNTs-PF-10cyc (e) and CNTs-10cyc (f).

## Conclusions

A highly efficient hydrogen-evolution electrode was successfully fabricated by PF-assisted CoPi amorphously electrodeposited onto PF-CNTs substrates through  $\pi$ - $\pi$  stacking interactions. The obtained CNTs-PF-10cyc electrocatalysts showed a low overpotential of  $105$  mV at a current density of  $10$   $\text{mA}\cdot\text{cm}^{-2}$  and a small Tafel slope of  $32$   $\text{mV}\cdot\text{dec}^{-1}$ , suggesting excellent electrocatalytic activity for the HER. The as-prepared CNTs-PF-10cyc catalytic electrode provided a large ECSA for quick transport of electrons and ions. Stability tests indicated that the CNTs-PF-10cyc catalysts could operate for at least  $24$  h with almost no current attenuation. The improved properties derived from creating a more uniform structure of CoPi on CNTs via small molecule functionalization could give rise to a new approach for designing and constructing efficient HER catalysts.

## Experimental

### Materials

Cobalt sulfate heptahydrate (AR, 99.5%), sodium hypophosphite (AR 99%), boric acid (AR, 99.5%) and tris(4-fluorophenyl)phosphine (PF) (AR, 99%) were purchased from Aladdin. The molecular structural formula of PF is shown in Figure S1. The raw carbon nanotubes (raw CNTs) were purchased from Cnano Technology (Beijing) Limited Company. All chemicals were used without further purification. The water ( $18.2$   $\text{M}\Omega\cdot\text{cm}^{-1}$ ) used in all experiments was prepared through an ultra-pure purification system.

### Electrode preparation

GCEs were polished in  $0.3$  and  $0.05$   $\mu\text{m}$  alumina slurry (CH Instrument Inc.). The electrodes were subsequently sonicated in ultrapure water and ethanol, and dried under a gentle nitrogen stream. To prepare the working electrode,  $3$  mg of CNTs and  $1$  mg of PF were ultrasonically dispersed in  $1000$   $\mu\text{L}$  of ethanol and deionized water (the volume ratio of ethanol and deionized water is  $4 : 1$ ). The precursor solution was prepared by mixing CNTs with PF, then  $8$   $\mu\text{L}$  of the resulting suspension was dropped onto the surface of GCEs and dried naturally at room temperature, which obtained PF-CNTs-modified GCE. For comparison, a commercially available Pt/C-modified GCE ( $20$  wt% Pt supported on carbon black) was prepared in the same process.

### Synthesis of CoPi/PF-CNTs nanocomposites

CoPi/PF-CNTs nanocomposites were synthesized by a facile electrochemical deposition method. Briefly, the PF-CNTs-modified GCEs were immersed in 0.3 mol/L  $\text{CoSO}_4 \cdot 7\text{H}_2\text{O}$  and  $\text{NaH}_2\text{PO}_4 \cdot \text{H}_2\text{O}$  solution containing  $\text{H}_3\text{BO}_3$ , and performed in the potential range from  $-1.8$  to  $+0.5$  V through cyclic voltammograms (CV) at a scan rate of 50 mV/s. After the electrochemical deposition, the working electrode was gently rinsed with water and dried overnight at room temperature. In our experiment, all of the potentials are calibrated based on reversible hydrogen electrode (RHE) according to the Nernst equation. For comparison, bare GCE and the CNTs-modified GCE were also treated under the same synthesis conditions, and parallel experiments using various deposition cycles and precursor concentrations were also systematically optimized. The obtained hybrids were denoted as CNTs-PF, CNTs-PF-5cyc, CNTs-PF-10cyc, CNTs-PF-20cyc, CNTs-10cyc, bare-10cyc, and so on. The preparations of catalyst materials with different concentration (0.15, 0.45 mol/L) of solution are also used as the control experiments.

### Structure characterization

X-ray photoelectron spectroscopy (XPS) measurements were carried out with an ultrahigh-vacuum setup, equipped with a monochromatic Al K $\alpha$  X-ray source and a high resolution Gamdata-Scienta SES 2002 analyzer. SEM images were obtained with a FEI Nova Nano SEM 200. TEM, high-resolution transmission electron microscopy (HRTEM), STEM and corresponding elemental mapping were recorded with a JEOL-2100F instrument.

### Electrochemical measurements

All electrochemical measurements, including cyclic voltammograms (CVs) and linear sweep voltammograms (LSVs) were performed at room temperature in a three-electrode system on CHI760 electrochemical workstation (CH Instrument Inc.). A PF-CNTs-modified GCE was used as the working electrode, a graphite electrode as counter electrode, and a Ag/AgCl (saturated-KCl) electrode as reference electrode. The Ag/AgCl reference electrode was calibrated with respect to reversible hydrogen electrode (RHE) for the measurements. The polarization curves were corrected for the ohmic potential drop ( $iR$ ) losses and the potentials reported in our work were obtained vs the reversible hydrogen electrode (RHE),  $E(\text{vs. RHE}) = E(\text{vs. Ag/AgCl}) + 0.226 + 0.059 \text{ pH}$  in 0.5 mol/L  $\text{H}_2\text{SO}_4$ . LSV was recorded in 0.5 mol/L  $\text{H}_2\text{SO}_4$  solutions at a scan rate of 5  $\text{mV} \cdot \text{s}^{-1}$  to obtain the polarization curves. The chronoamperometry ( $i-t$ ) curves were recorded over 24 h at  $\eta = 100$  mV in 0.5 mol/L  $\text{H}_2\text{SO}_4$ . The ECSA was determined by measuring the capacitive current associated with double-layer charging from the scan-rate dependence of CV. The CVs taken with various scan rates (20, 40, 80, 160, 200  $\text{mV} \cdot \text{s}^{-1}$ , etc.) were used under the potential window of 0–0.3 V vs RHE. The Tafel plots were obtained from LSV curves for assessment of the HER activities of investigated catalysts. According to the Tafel equation ( $\eta = b \log j + a$ ), the Tafel slope ( $b$ ) can be obtained by fitting the linear portion of the Tafel plots to it. EIS measurement was performed in 5 mmol/L  $\text{H}_2\text{SO}_4$  over a frequency range from 100 kHz to 0.01 Hz at a bias potential of 100 mV (vs. RHE).

### Supporting Information

The supporting information for this article is available on the WWW under <https://doi.org/10.1002/cjoc.202100695>.

### Acknowledgement

The work was supported in part by grants from the Natural Science Foundation of Zhejiang Province (No. LR18E020001), the

National Natural Science Foundation of China (Nos. 51972238, 21875166), and the Science and Technology Project of Zhejiang Province (No. LGF18B050005)

### References

- [1] Gong, Q.; Wang, Y.; Hu, Q.; Zhou, J.; Feng, R.; Duchesne, P. N.; Zhang, P.; Chen, F.; Han, N.; Li, Y.; Jin, C.; Li, Y.; Lee, S. T. Ultrasmall and Phase-Pure  $\text{W}_2\text{C}$  Nanoparticles for Efficient Electrocatalytic and Photoelectrochemical Hydrogen Evolution. *Nat. Commun.* **2016**, *7*, 13216.
- [2] Liu, X.; Dai, L. Carbon-Based Metal-Free Catalysts. *Nat. Rev. Mater.* **2016**, *1*, 16064.
- [3] Kim, H.; Hwang, E.; Park, H.; Lee, B. S.; Jang, J. H.; Kim, H. J.; Ahn, S. H.; Kim, S. K. Non-Precious Metal Electrocatalysts for Hydrogen Production in Proton Exchange Membrane Water Electrolyzer. *Appl. Catal. B: Environ.* **2017**, *206*, 608–616.
- [4] Zhu, X.; Tang, C.; Wang, H. F.; Li, B. Q.; Zhang, Q.; Li, C.; Yang, C.; Wei, F. Monolithic-Structured Ternary Hydroxides as Freestanding Bifunctional Electrocatalysts for Overall Water Splitting. *J. Mater. Chem. A* **2016**, *4*, 7245–7250.
- [5] Li, P.; Yang, Z.; Shen, J.; Nie, H.; Cai, Q.; Li, L.; Ge, M.; Gu, C.; Chen, X.; Yang, K.; Zhang, L.; Chen, Y.; Huang, S. Subnanometer Molybdenum Sulfide on Carbon Nanotubes as A Highly Active and Stable Electrocatalyst for Hydrogen Evolution Reaction. *ACS Appl. Mater. Inter.* **2016**, *8*, 3543–3550.
- [6] Zhang, L.; Han, L.; Liu, H.; Liu, X.; Luo, J. Potential-Cycling Synthesis of Single Platinum Atoms for Efficient Hydrogen Evolution in Neutral Media. *Angew. Chem. Int. Ed.* **2017**, *56*, 13694–13698.
- [7] Tang, K.; Wang, X.; Li, Q.; Yan, C. High Edge Selectivity of in Situ Electrochemical Pt Deposition on Edge-Rich Layered  $\text{WS}_2$  Nanosheets. *Adv. Mater.* **2017**, *29*, 1704779.
- [8] Zhan, Y.; Li, Y.; Yang, Z.; Wu, X.; Ge, M.; Zhou, X.; Hou, J.; Zheng, X.; Lai, Y.; Pang, R.; Duan, H.; Chen, X.; Nie, H.; Huang, S. Synthesis of a  $\text{MoS}_x\text{-O-PtO}_x$  Electrocatalyst with High Hydrogen Evolution Activity Using a Sacrificial Counter-Electrode. *Adv. Sci.* **2019**, *6*, 1801663.
- [9] Lv, H.; Xi, Z.; Chen, Z.; Guo, S.; Yu, Y.; Zhu, W.; Li, Q.; Zhang, X.; Pan, M.; Lu, G.; Mu, S.; Sun, S. A New Core/Shell NiAu/Au Nanoparticle Catalyst with Pt-Like Activity for Hydrogen Evolution Reaction. *J. Mater. Chem. A* **2015**, *137*, 5859–5862.
- [10] Feng, J.; Lv, F.; Zhang, W.; Li, P.; Wang, K.; Yang, C.; Wang, B.; Yang, Y.; Zhou, J.; Lin, F.; Wang, G. C.; Guo, S. Iridium-based Multimetallic Porous Hollow Nanocrystals for Efficient Overall-Water-Splitting Catalysis. *Adv. Mater.* **2017**, *29*, 1703798.
- [11] Huang, Y.; Gong, Q.; Song, X.; Feng, K.; Nie, K.; Zhao, F.; Wang, Y.; Zeng, M.; Zhong J.; Li, Y.  $\text{Mo}_2\text{C}$  Nanoparticles Dispersed on Hierarchical Carbon Microflowers for Efficient Electrocatalytic Hydrogen Evolution. *ACS Nano* **2016**, *10*, 11337–11343.
- [12] Zhang, J.; Qu, L.; Shi, G.; Liu, J.; Chen, J.; Dai, L. N,P-Codoped Carbon Networks as Efficient Metal-Free Bifunctional Catalysts for Oxygen Reduction and Hydrogen Evolution Reactions. *Angew. Chem. Int. Ed.* **2016**, *55*, 2230–2234.
- [13] Ma, L.; Hu, Y.; Zhu, G.; Chen, R.; Chen, T.; Lu, H.; Wang, Y.; Liang, J.; Liu, H.; Yan, C.; Tie, Z.; Jin Z.; Liu, J. In Situ Thermal Synthesis of Inlaid Ultrathin  $\text{MoS}_2$ /Graphene Nanosheets as Electrocatalysts for the Hydrogen Evolution Reaction. *Chem. Mater.* **2016**, *28*, 5733–5742.
- [14] Zhan, Y.; Zhou, X.; Nie, H.; Xu, X.; Zheng, X.; Hou, J.; Duan, H.; Huang, S.; Yang, Z. Designing Pd/O Co-Doped  $\text{MoS}_x$  for Boosting the Hydrogen Evolution Reaction. *J. Mater. Chem. A* **2019**, *7*, 15599–15606.
- [15] Ma, R.; Song, E.; Zhou, Y.; Zhou, Z.; Liu, G.; Liu, Q.; Liu, J.; Zhu, Y.; Wang, J. Ultrafine WC Nanoparticles Anchored on Co-Encased, N-Doped Carbon Nanotubes for Efficient Hydrogen Evolution. *Energy Storage Mater.* **2017**, *6*, 104–111.
- [16] Zhang, Z.; Yi, Z.; Wang, J.; Tian, X.; Xu, P.; Shi, G.; Wang, S. Nitrogen-Enriched Polydopamine Analogue-Derived Defect-Rich Porous Carbon as a Bifunctional Metal-Free Electrocatalyst for Highly Efficient

- Overall Water Splitting. *J. Mater. Chem. A* **2017**, *5*, 17064–17072.
- [17] Weng, Z.; Liu, W.; Yin, L. C.; Fang, R.; Li, M.; Altman, E. I.; Fan, Q.; Li, F.; Cheng, H. M.; Wang, H. Metal/Oxide Interface Nanostructures Generated by Surface Segregation for Electrocatalysis. *Nano Lett.* **2015**, *15*, 7704–7710.
- [18] Xiao, Z.; Wang, Y.; Huang, Y. C.; Wei, Z.; Dong, C. L.; Ma, J.; Shen, S.; Li, Y.; Wang, S. Filling the Oxygen Vacancies in  $\text{Co}_3\text{O}_4$  with Phosphorus: an Ultra-Efficient Electrocatalyst for Overall Water Splitting. *Energy Environ. Sci.* **2017**, *10*, 2563–2569.
- [19] Jing, S.; Zhang, L.; Luo, L.; Lu, J.; Yin, S.; Shen, P. K.; Tsiakaras, P. N-Doped Porous Molybdenum Carbide Nanobelts as Efficient Catalysts for Hydrogen Evolution Reaction. *Appl. Catal. B: Environ.* **2018**, *224*, 533–540.
- [20] Gao, W.; Yan, M.; Cheung, H. Y.; Xia, Z.; Zhou, X.; Qin, Y.; Wong, C. Y.; Ho, J. C.; Chang, C. R.; Qu, Y. Modulating Electronic Structure of CoP Electrocatalysts Towards Enhanced Hydrogen Evolution by Ce Chemical Doping in Both Acidic and Basic Media. *Nano Energy* **2017**, *38*, 290–296.
- [21] Li, W.; Zhang, S.; Fan, Q.; Zhang, F.; Xu, S. Hierarchically Scaffolded CoP/CoP<sub>2</sub> Nanoparticles: Controllable Synthesis and Their Application as a Well-Matched Bi-Functional Electrocatalyst for Overall Water Splitting. *Nanoscale* **2017**, *9*, 5677–5685.
- [22] Zheng, X.; Nie, H.; Zhan, Y.; Zhou, X.; Duan, H.; Yang, Z. Intermolecular Electron Modulation by P/O Bridging in an IrO<sub>2</sub>-CoPi Catalyst to Enhance the Hydrogen Evolution Reaction. *J. Mater. Chem. A* **2020**, *8*, 8273–8280.
- [23] Xiao, X.; He, C.; Zhao, S.; Li, J.; Lin, W.; Yuan, Z.; Zhang, Q.; Wang, S.; Dai, L.; Yu, D. A General Approach to Cobalt-Based Homobimetallic Phosphide Ultrathin Nanosheets for Highly Efficient Oxygen Evolution in Alkaline Media. *Energy Environ. Sci.* **2017**, *10*, 893–899.
- [24] Gonzalez-Flores, D.; Sanchez, I.; Zaharieva, I.; Klingan, K.; Heidkamp, J.; Chernev, P.; Menezes, P. W.; Driess, M.; Dau, H.; Montero, M. L. Heterogeneous Water Oxidation: Surface Activity versus Amorphization Activation in Cobalt Phosphate Catalysts. *Angew. Chem. Int. Ed.* **2015**, *54*, 2472–2476.
- [25] Sun, X.; Huo, J.; Yang, Y.; Xu, L.; Wang, S. The  $\text{Co}_3\text{O}_4$  Nanosheet Array as Support for  $\text{MoS}_2$  as Highly Efficient Electrocatalysts for Hydrogen Evolution Reaction. *J. Energy Chem.* **2017**, *26*, 1136–1139.
- [26] Popczun, E. J.; Roske, C. W.; Read, C. G.; Crompton, J. C.; McEnaney, J. M.; Callejas, J. F.; Lewis, N. S.; Schaak, R. E. Highly Branched Cobalt Phosphide Nanostructures for Hydrogen-Evolution Electrocatalysis. *J. Mater. Chem. A* **2015**, *3*, 5420–5425.
- [27] Cobo, S.; Heidkamp, J.; Jacques, P. A.; Fize, J.; Fourmond, V.; Guetaz, L.; Jusselme, B.; Ivanova, V.; Dau, H.; Palacin, S.; Fontecave, M.; Artero, V. A Janus Cobalt-Based Catalytic Material for Electro-Splitting of Water. *Nat. Mater.* **2012**, *11*, 802–807.
- [28] Pan, Y.; Su, K.; Liu, S.; Cao, X.; Wu, K.; Cheong, W.; Chen, Z.; Wang, Y.; Li, Y.; Liu, Y.; Wang, D.; Peng, Q.; Chen, C.; Li, Y. Core-Shell ZIF-8@ZIF-67-Derived CoP Nanoparticle-Embedded N-Doped Carbon Nanotube Hollow Polyhedron for Efficient Overall Water Splitting. *J. Am. Chem. Soc.* **2018**, *140*, 2610–2618.
- [29] Yang, J.; Guo, D.; Zhao, S.; Lin, Y.; Yang, R.; Xu, D.; Shi, N.; Zhang, X.; Lu, L.; Lan, Y.; Bao, J.; Han, M. Cobalt Phosphides Nanocrystals Encapsulated by P-Doped Carbon and Married with P-Doped Graphene for Overall Water Splitting. *Small* **2019**, *15*, 1804546.
- [30] Hoa, V.; Tran, D.; Le, H.; Kim, N.; Lee, J. Hierarchically porous nickel-cobalt phosphide nanoneedle arrays loaded micro-carbon spheres as an advanced electrocatalyst for overall water splitting application. *Appl. Catal. B-Environ.* **2019**, *253*, 235–245.
- [31] Bai, N.; Li, Q.; Mao, D.; Li, D.; Dong, H. One-Step Electrodeposition of Co/CoP Film on Ni Foam for Efficient Hydrogen Evolution in Alkaline Solution. *ACS Appl. Mater. Inter.* **2016**, *8*, 29400–29407.
- [32] Ye, C.; Wang, M.; Chen, G.; Deng, Y.; Li, L.; Luo, H.; Li, N. One-Step CVD Synthesis of Carbon Framework Wrapped  $\text{Co}_2\text{P}$  as Flexible Electrocatalyst for Efficient Hydrogen Evolution. *J. Mater. Chem. A* **2017**, *5*, 7791–7795.
- [33] Xu, K.; Ding, H.; Zhang, M.; Chen, M.; Hao, Z.; Zhang, L.; Wu, C.; Xie, Y. Regulating Water-Reduction Kinetics in Cobalt Phosphide for Enhancing HER Catalytic Activity in Alkaline Solution. *Adv. Mater.* **2017**, *29*, 1606980.
- [34] Shen, J.; Yang, Z.; Ge, M.; Li, P.; Nie, H.; Cai, Q.; Gu, C.; Yang, K.; Huang, S. Neuron-Inspired Interpenetrative Network Composed of Cobalt-Phosphorus-Derived Nanoparticles Embedded within Porous Carbon Nanotubes for Efficient Hydrogen Production. *ACS Appl. Mater. Inter.* **2016**, *8*, 17284–17291.
- [35] Yang, F.; Chen, Y.; Cheng, G.; Chen, S.; Luo, W. Ultrathin Nitrogen-Doped Carbon Coated with CoP for Efficient Hydrogen Evolution. *ACS Catal.* **2017**, *7*, 3824–3831.
- [36] Xu, G. R.; Bai, J.; Yao, L.; Xue, Q.; Jiang, J. X.; Zeng, J. H.; Chen, Y.; Lee, J. M. Polyallylamine-Functionalized Platinum Tripods: Enhancement of Hydrogen Evolution Reaction by Proton Carriers. *ACS Catal.* **2017**, *7*, 452–458.
- [37] Charlier, J. C.; Ebbesen, T. W.; Lambin, P. Structural and Electronic Properties of Pentagon-Heptagon Pair Defects in Carbon Nanotubes. *Phys. Rev. B* **1996**, *53*, 11108–11113.
- [38] Lai, Y.; Nie, H.; Xu, X.; Fang, G.; Ding, X.; Chan, D.; Zhou, S.; Zhang, Y.; Chen, X.; Yang, Z. Interfacial Molecule Mediators in Cathodes for Advanced Li-S Batteries. *ACS Appl. Mater. Inter.* **2019**, *11*, 29978–29984.
- [39] Song, J.; Zhu, C.; Xu, B. Z.; Fu, S.; Engelhard, M. H.; Ye, R.; Du, D.; Beckman, S. P.; Lin, Y. Bimetallic Cobalt-based Phosphide Zeolitic Imidazolate Framework: CoP<sub>x</sub> Phase-Dependent Electrical Conductivity and Hydrogen Atom Adsorption Energy for Efficient Overall Water Splitting. *Adv. Energy Mater.* **2017**, *7*, 1601555.
- [40] Wang, A. L.; Lin, J.; Xu, H.; Tong, Y. X.; Li, G. R. Ni<sub>2</sub>P-CoP Hybrid Nanosheet Arrays Supported on Carbon Cloth as an Efficient Flexible Cathode for Hydrogen Evolution. *J. Mater. Chem. A* **2016**, *4*, 16992–16999.
- [41] Tang, C.; Gan, L.; Zhang, R.; Lu, W.; Jiang, X.; Asiri, A. M.; Sun, X.; Wang, J.; Chen, L. Ternary Fe<sub>x</sub>Co<sub>1-x</sub>P Nanowire Array as a Robust Hydrogen Evolution Reaction Electrocatalyst with Pt-like Activity: Experimental and Theoretical Insight. *Nano Lett.* **2016**, *16*, 6617–6621.
- [42] Li, Y.; Wang, H.; Xie, L.; Liang, Y.; Hong, G.; Dai, H.  $\text{MoS}_2$  Nanoparticles Grown on Graphene: an Advanced Catalyst for the Hydrogen Evolution Reaction. *J. Am. Chem. Soc.* **2011**, *133*, 7296–7299.
- [43] Yang, J.; Yang, Z.; Li, L.; Cai, Q.; Nie, H.; Ge, M.; Chen, X.; Chen, Y.; Huang, S. Highly Efficient Oxygen Evolution from  $\text{CoS}_2/\text{CNTs}$  Nanocomposite via One-Step Electrochemical Deposition and Dissolution Method. *Nanoscale* **2017**, *9*, 6886–6894.

Manuscript received: December 30, 2020

Manuscript revised: March 28, 2021

Manuscript accepted: April 13, 2021

Accepted manuscript online: April 15, 2021

Version of record online: XXXX, 2021